

Proton elastic scattering on light nuclei. I. Energy dependence

E. Fabrici, S. Micheletti, M. Pignanelli, and F. G. Resmini

Istituto di Fisica dell'Università di Milano and Istituto Nazionale di Fisica Nucleare, Sezione di Milano, Milano, Italy

R. De Leo, G. D'Erasmus, and A. Pantaleo

Istituto di Fisica dell'Università di Bari and Istituto Nazionale di Fisica Nucleare, Sezione di Bari, Bari, Italy

J. L. Escudé and A. Tarrats

Département de Physique Nucléaire, CEN Saclay, BP 2, 91190 Gif-sur-Yvette, France

(Received 22 June 1979)

Differential cross sections for proton elastic scattering by ^{15}N , ^{18}O , ^{24}Mg , and ^{40}Ar were measured at several proton energies between 14 and 44 MeV. Previous data on ^{12}C , ^{16}O , ^{24}Mg , ^{28}Si , and ^{40}Ca have also been considered. Evidence has been found for a strong enhancement in proton emission at backward angles for scattering by spherical nuclei at incident energies higher than 26 MeV. A phase-shift analysis of all the differential cross sections showed that the partial waves involved are those near grazing. Optical-model fits of good quality have been obtained for collective nuclei, while for spherical nuclei the cross sections at backward angles are not reproduced. The disagreement is not substantially modified when nonstandard radial dependences are given to the optical potential.

NUCLEAR REACTIONS Proton elastic scattering on ^{15}N , $E_p = 18.1\text{--}44.2$ MeV; ^{18}O , $E_p = 14.7\text{--}44.1$ MeV; ^{24}Mg , $E_p = 35.2\text{--}44.1$ MeV; ^{40}Ar , $E_p = 20.9\text{--}44.1$ MeV. Measured $\sigma(\theta)$. Comparison with phase-shift and optical-model analysis. Deduced optical-model potentials.

I. INTRODUCTION

For incident nucleon energies above 20 MeV the optical model has been shown to give a satisfactory description of elastic scattering on heavy and medium-weight nuclei.¹ This model has not enjoyed the same success in its application to light nuclei. Published systematic studies involve mainly proton scattering at energies up to 30 MeV. While any single angular distribution can be reproduced, the optical-model parameters required for different energies very often display marked fluctuations. This behavior may indicate that resonant processes are important for light nuclei also in the 20–30 MeV energy range.^{2–10}

For some nuclei the agreement between experiment and calculation improves at higher energies, although this is not true for doubly magic nuclei such as ^{16}O and ^{40}Ca . For the latter, in 1967 Gross *et al.*¹¹ had already shown that in the 30–45 MeV range it is impossible to fit the cross section at backward angles with standard sets of optical-model parameters. The same authors also showed that it is very difficult to obtain fits simultaneously to both the polarization and the cross section and that the quality of the fits can be easily improved by making only a slight adjustment in the reflection coefficient associated with the grazing partial waves. Moreover the phase shifts resulting from

their analysis give no indication of resonant processes.

Most of the exhaustive elastic scattering studies have been motivated by the search for average optical-model potentials suitable for nuclear reaction calculations. Even at fairly high excitations the level density for light nuclei is low and hence nuclear structure effects are not sufficiently averaged out. Consequently it was commonly accepted that resonance effects could be present and that they should be more important at those angles for which the potential scattering is small. Therefore in the analyses whose goal was the extraction of average potentials, the quality of the fits obtained at backward angles was generally disregarded.^{4,12,13}

The recent progress made in folding model calculations of optical-model potentials^{14–16} and a better understanding of the role played by the coupling between elastic and reaction channels^{17,18} have stimulated renewed interest in more detailed knowledge of proton elastic scattering on light nuclei.

We decided to investigate the situation further by examining the following points: (i) The possibility that “unconventional” shapes of differential cross sections could be present for other nuclei besides the well known cases of ^{16}O and ^{40}Ca , (ii) the energy dependence of these “unconvention-

al" effects, and (iii) their correlation with any simple nuclear property.

This paper, hereafter referred to as I, concerns the energy dependence between 15 and 44 MeV of proton elastic scattering on a limited number of target nuclei with a mass number $A \leq 40$. An accompanying paper, referred to as II, will be devoted to proton elastic scattering mass dependence, between $A = 9$ and 70, at a fixed bombarding energy of 35.2 MeV.¹⁹ In these two papers special stress is laid on the phenomenological aspects resulting from the systematic measurements we have performed. The calculations, done in the framework of a conventional optical model, are used mostly as a reference in classifying the data. Moreover, to gain further insight into the problem, a phase-shift analysis was carried out on a substantial part of the data. Extensive comparison with more recent theories, such as folding model for optical potentials and the evaluation of two-step contributions, are the subject of a study now being done.

II. EXPERIMENTAL METHOD

The experiment was performed using the energy analyzed beam of the Milan sector-focused cyclotron. Where beams with energy between about 20 and 44 MeV were available, lower energies were obtained by means of Be absorbers placed in the first part of the beam channel. The 120° analyzing magnet allows energy resolutions $\Delta E/E$ up to $2-3 \times 10^{-4}$, although $\Delta E/E$ values of about 10^{-3} were typically used in these measurements.

The scattered protons were detected by silicon surface-barrier detectors, stacked in two or three counter telescopes placed on a plate cooled to about -5°C and rotated by remote controls. Both solid and gas targets were used. Solid target areal densities were determined by weighting method. The gas pressure was measured using a precision dial manometer with scale divisions of 0.005 kg/cm^2 and absolute accuracy of the same order. The gas pressure, generally about 0.5 kg/cm^2 , was corrected for the temperature variations. The gas cell consisted of a brass housing with a 1.8 mg/cm^2 thick Kapton foil window.

To ensure beam alignment with the counter setup, the same counter was routinely positioned on either side of the beam itself and the counting rates for elastically scattered protons were compared. The overall energy resolution, which includes the counter resolution, the incident beam energy spread, the kinematic broadening and the effect of target thickness, varied from 70 to 100 keV depending mainly on target thickness. The overall angular resolution varied from $\pm 0.3^\circ$ to

$\pm 0.9^\circ$ for the different slit systems used for solid and gas targets and for the different telescopes. Solid angles varied from $4 \cdot 10^{-5}$ to $6 \cdot 10^{-4}$ sr.

Differential cross sections were measured at 13 incident energies between 18 and 44 MeV for ^{15}N , at 16 energies between 14 and 44 MeV for ^{18}O and at 9 energies between 20 and 44 MeV for ^{40}Ar . Data were collected at scattering angles from $10^\circ-15^\circ$ to $165^\circ-170^\circ$ in steps of about 5° . Gas targets were used for these nuclei; ^{15}N and ^{18}O gases were isotopically enriched to 95%. Previous data⁸ on ^{24}Mg were supplemented in this experiment by further measurements in the energy range 35–44 MeV. In the latter case a solid target 1.03 mg/cm^2 thick and enriched to 99.9%, was used.

The uncertainty in absolute cross section values was estimated to be about 4%. Statistical errors were generally negligible. A more detailed discussion of the errors affecting the present measurements is given in paper II. Numerical data on differential cross sections reported here and in paper II together with further details on the experiment are given elsewhere.²⁰

III. EXPERIMENTAL FEATURES OF THE DATA

The data considered in the following, which have been taken also from previous studies,^{6-8,10,11,21-34} are listed in Table I. Besides those collected in this experiment the most relevant are those given by Gross *et al.*¹¹ and van Oers¹³ for ^{40}Ca and by some of us for ^{12}C , ^{15}N , ^{18}O , ^{24}Mg , and ^{28}Si .^{6,8,10,23,25} Other studies on ^{12}C and ^{16}O have been also taken into account.^{4,5}

The new measurements¹⁹ at 35.2 MeV on ^{12}C , ^{16}O , ^{24}Mg , ^{28}Si , and ^{40}Ca constitute a useful test of the agreement between the present and previous measurements taken at our laboratory and others. The polarization data, when available, have also been considered. Although taken into account only at some incident energies, these data provide a valid tool when reducing the ambiguities of best fit procedures in optical-model and phase-shift analyses.

The above target nuclei were selected in order to have systematic data for elastic cross section energy dependence on four spherical nuclei (^{15}N , ^{16}O , ^{40}Ar , and ^{40}Ca), on a slightly collective nucleus (^{18}O), on a deformed nucleus (^{28}Si) and on two strongly deformed nuclei (^{12}C and ^{24}Mg). In fact, during this study it immediately became apparent that collective properties are indeed a sensible index for classifying the target nuclei with respect to the effects studied here.

The differential cross sections for proton elastic scattering on ^{15}N , ^{18}O , ^{24}Mg , ^{40}Ar , and ^{40}Ca

TABLE I. Data selection for proton elastic scattering optical-model analysis.

Nucleus	Incident energies for cross sections (MeV)	Incident energies for polarizations (MeV)
^{12}C	(15.9-17.35-18.5-20.0-22.65-24.65-26.1-27.3-28.85-29.9-33.15-35.3) ^a -40.0 ^b	(20.2-22.6-24.1-26.2-27.1-28.3) ^c -40.0 ^b
^{15}N	18.1-20.0-(22.4-24.5-26.0) ^d -28.1-30.0-32.1-35.2-37.1-39.2-41.7-44.2	(22.4-24.5-26.0) ^d
^{18}O	14.7-16.3 ^e -17.7-19.1-20.6-22.3-(22.5-24.5) ^f -26.2-28.2-30.5-32.76-35.2-37.3-39.5-41.4-44.1	(22.5-24.5) ^f
^{24}Mg	(15.5-16.5-17.2-18.5-19.5-20.5-21.6-22.5-23.6) ^g -25.2 ^h -26.5 ^g -30.5 ⁱ -35.2-39.5-44.1-49.5 ^j	17.5 ^k -20.3 ^l -49.5 ^j
^{28}Si	(14.26-15.34-15.83-16.3-16.8-17.24-17.67-18.18-18.73-19.23-19.7-20.17-21.32-22.7-23.6-24.24-25.44-26.34-27.3-28.7-29.47-30.5-31.5-32.4-33.7-34.7) ^m -35.2-(35.97-37.21-38.6-40.21) ^m	20.3 ^l -25.2 ⁿ -30.3 ^o
^{40}Ar	20.9-23.5-26.3-29.3-30.4 ^p -32.2-35.2-38.2-40.7-44.1-49.4 ^p	(30.4-49.4) ^p
^{40}Ca	(21.1-23.5-26.3-48.0) ^q -30.3 ^r -35.2-(35.8-40.0-45.5) ^r	26.3 ^s -(30.3-35.8-40.0-45.5) ^r

^a Reference 6.^b Reference 21.^c Reference 22.^d Reference 23.^e Reference 24.^f Reference 25.^g Reference 8.^h Reference 7.ⁱ Reference 26.^j Reference 27.^k Reference 28.^l Reference 29.^m Reference 10.ⁿ Reference 30.^o Reference 31.^p Reference 32.^q Reference 33.^r Reference 11.^s Reference 34.

are given in Figs. 1 to 5. To show the energy dependence of the diffraction pattern more clearly the angular distributions were drawn displaced proportionally to energy increments. The curves given in these figures are the result of a phase-shift analysis (see Sec. VI). Equivalent comprehensive figures are given in Refs. 5 and 6 for ^{12}C and in Ref. 4 for ^{16}O .

The evolution of the diffraction pattern becomes fairly regular above 25 MeV. In the case of ^{15}N , $^{16,18}\text{O}$, ^{40}Ar , and ^{40}Ca , a pronounced maximum at angles larger than 140° which stands out from the pattern appears at about 25–26 MeV. This maximum is still present at 44 MeV for ^{15}N and ^{18}O and has been evidenced for ^{16}O up to 52 MeV.⁴ It seems to disappear between 40 and 45 MeV in the cases of ^{40}Ar and ^{40}Ca . It is difficult to indicate an upper energy limit for this backward enhancement due partly to lack of data and partly to the fact that the above maximum disappears slowly at high energy and probably merges into another maximum which, at least for ^{40}Ar at 44.1 MeV, looks like a normal maximum in the diffraction pattern (Fig. 7).

To evaluate the lower limit more clearly, the angular position of the above maximum can be plotted against the incident energy. These plots are given in Fig. 6; data for ^{14}N have also been

included.^{19,32,35} The maximum shifts rapidly towards larger angles at the energies at which it appears or is still increasing and stays practically fixed after that. This trend is probably the main cause of the failure of conventional optical-model calculations to reproduce differential cross sections at incident energies above 25–30 MeV for many light nuclei. In fact, in the region in which the backward peak changes rapidly in the angular position, attempts to fit the full angular distribution lead to corresponding abrupt large variations in both the geometrical parameters and the well depths. This contrasts with the uniform slow variations of the same parameters with the incident energy which are expected in the optical model. The dashed lines on the ^{40}Ca data in Fig. 6 show the peak position energy dependence predicted by an optical-model calculation. A more detailed comparison with optical-model predictions will be given in the next section.

For the medium collective nucleus ^{28}Si , a backward peak with the energy dependence of the type described above appears, with a very limited magnitude, only around 33–34 MeV (Fig. 7), the energy at which the effect is the largest for other nuclei. For ^{12}C (Figs. 1 and 2 of Refs. 5 and 6, respectively) and for the other strongly collective nucleus ^{24}Mg (Fig. 3) the backward effect has not

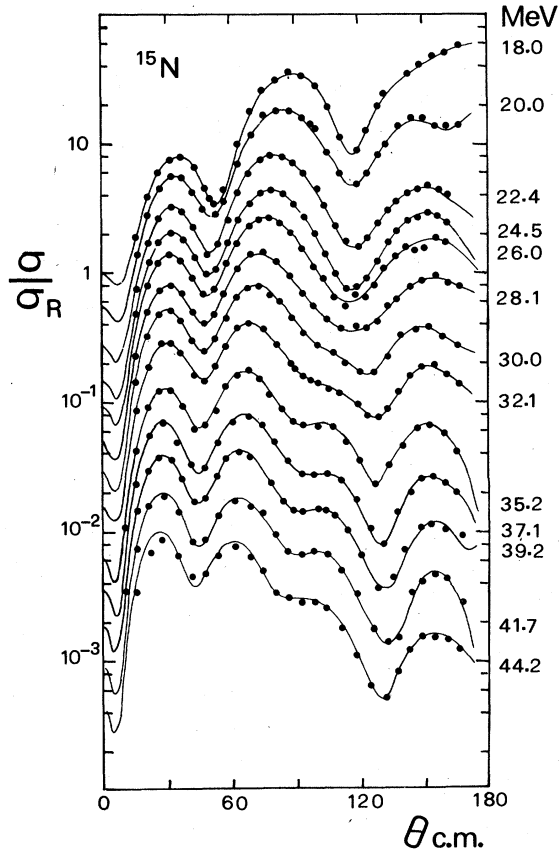


FIG. 1. Differential cross sections (points) for protons elastically scattered from ^{15}N , together with the results of a phase shift analysis (solid lines). The angular distributions are drawn displaced vertically in proportion to incident energy increments. True cross-section values are obtained by multiplying by $\exp[0.296(E_p - 18)]$.

been found.

A concluding remark is therefore that for all the spherical or slightly deformed nuclei, but for these nuclei only, an enhanced yield appears at backward angles at about the same incident energy, that is at 25–26 MeV, becoming clearly evident between 30 and 40 MeV.

IV. OPTICAL-MODEL ANALYSIS

The data have been analyzed in terms of the optical model, to help evidence their typical behavior. The analysis was done using the SNOOPY code which allows a best-fitting procedure by adjustment of the optical-model parameters or, directly, of the phase shifts. The optical potential was of a conventional type, i.e., local and with standard radial dependence:

$$V(r) = -V_0 f(x_0) - iW_{v0} f(x_w) + 4iW_D (d/dx_w) f(x_w) + V_c(r, R_c) + V_{so} (\hbar/m_p c)^2 (1/r) (d/dr) f(x_{so}),$$

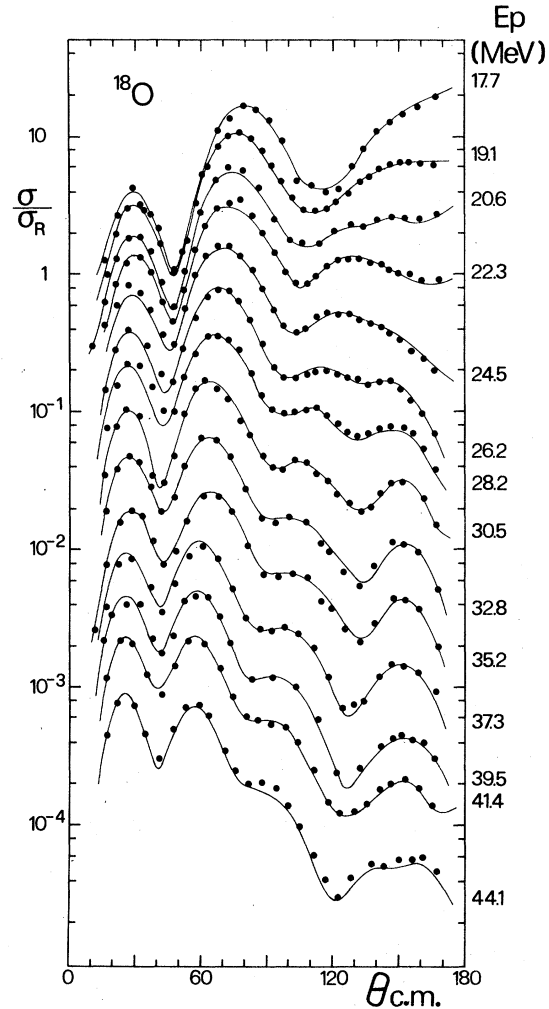


FIG. 2. Differential cross sections for proton elastic scattering on ^{18}O ; see caption for Fig. 1. The normalization factor is $\exp[0.37(E_p - 17.7)]$.

where $f(x_i)$, with $x_i = (r - R_i A^{1/3})/a_i$, are Woods-Saxon form factors and V_c is the Coulomb potential of a uniformly charged sphere of radius $R_c A^{1/3}$.

Owing to the above mentioned difficulties in fitting the complete angular distributions, only data up to an angle (generally 100° – 120°) were chosen in order to remove the backward maximum from the search. Compound nucleus contributions are expected to be largest for light nuclei at low energies. Hauser and Feshbach cross sections were evaluated at 16 MeV for ^{12}C and found a factor of 10 lower than the experiment at the most unfavorable angles. This factor increases with energy and target mass.^{8,10} These contributions have therefore been disregarded in the subsequent an-

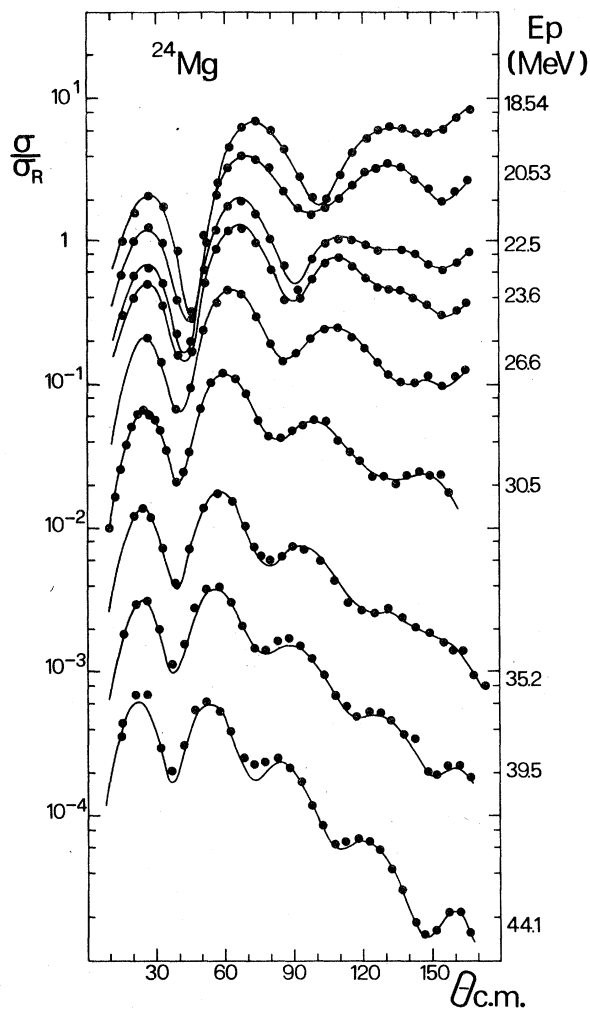


FIG. 3. Differential cross sections for proton elastic scattering on ^{24}Mg ; see caption for Fig. 1. The normalization factor is $\exp[0.37(E_p - 18.54)]$.

analysis. The fitting procedure was started by allowing all the optical-model parameters to be routinely in search in groups of 4 or 5. Emphasis was placed on obtaining good quality fits by using parameters with a smooth energy dependence. As a consequence of the nonlocality of the optical-model potentials, the geometries of the local-equivalent potentials are known to be energy dependent.^{12,14,15} However, over the energy interval considered, the predicted variations are probably too small to be determined directly from the experiment, also because several geometrical parameters are correlated to the well depths, which are more strongly energy dependent. For these reasons and also because no clear cut evidence to the contrary has been found, we chose energy-

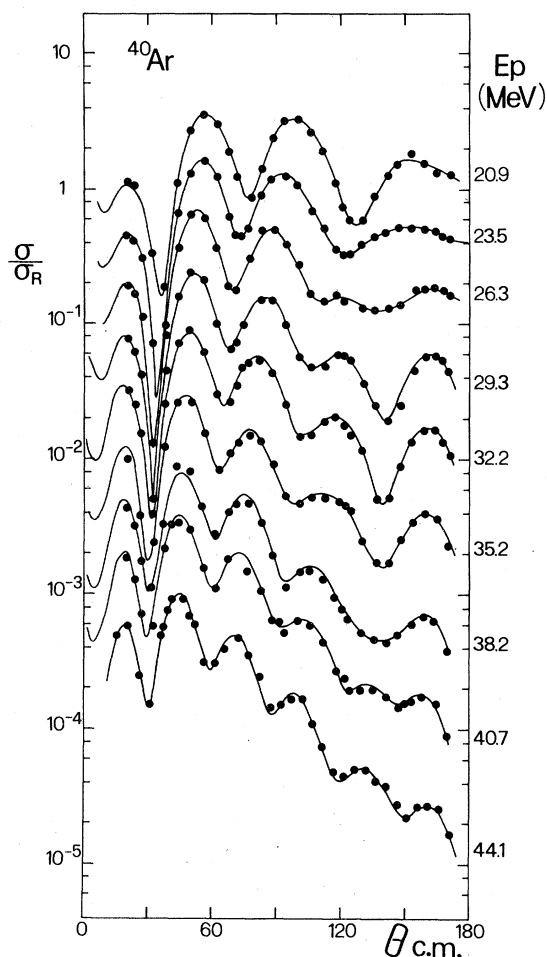


FIG. 4. Differential cross sections for proton elastic scattering on ^{40}Ar ; see caption for Fig. 1. The normalization factor is $\exp[0.37(E_p - 20.9)]$.

independent average values for the radius and diffuseness parameters. The spin-orbit strength was fixed considering polarization data.

The energy-dependent average potentials thus obtained are given in Table II. For comparison the χ^2 values obtained using previous^{5,8,10,13,36} energy-averaged potentials are also given in the last two columns. These are generally larger especially in the angular range considered in the search. The potentials obtained for ^{12}C and ^{40}Ca are almost equal to those determined in Refs. 5 and 11, respectively. In the case of collective nuclei, such as ^{12}C , ^{24}Mg , and ^{28}Si , the quality of the fits can sometimes be very poor at low energies, where contributions coming from resonant processes are evident,⁶⁻¹⁰ although it becomes satisfactory above 30 MeV. These potentials, deduced mainly from cross section data at forward

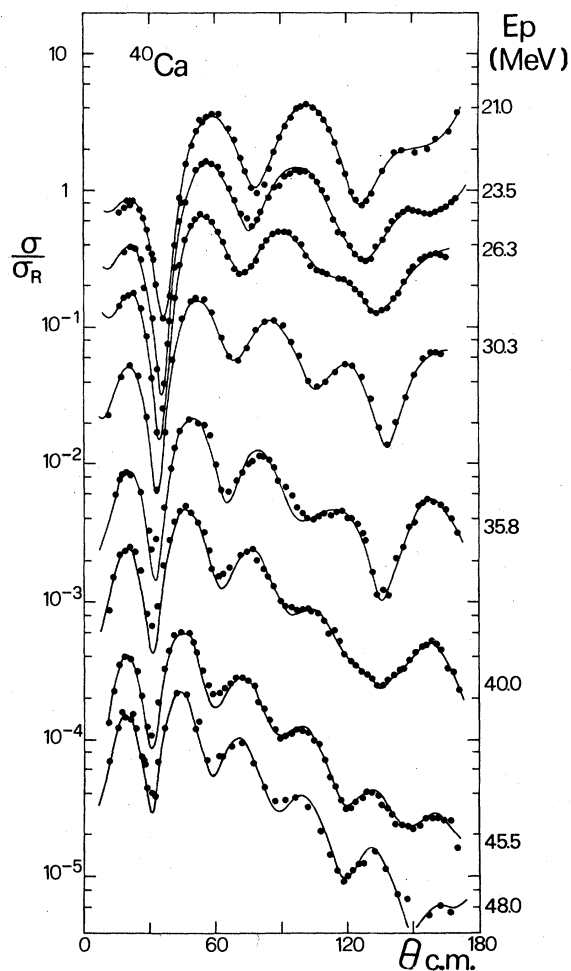


FIG. 5. Differential cross sections for proton elastic scattering on ^{40}Ca ; see caption for Fig. 1 and Table I. The normalization factor is $\exp[0.37(E_p - 21.0)]$.

angles, also correctly reproduce the polarization data and the cross sections at backward angles (Fig. 8). In the case of spherical or slightly deformed nuclei, such as ^{15}N , ^{18}O , ^{40}Ar , and ^{40}Ca , acceptable fits at backward angles are obtained for polarizations but not for cross sections (Fig. 9).

The potentials in Tables II show several features similar to those obtained in conventional¹ optical-model analyses of heavier nuclei, as may be seen especially by comparing global properties, such as root mean square radii or volume integrals for the different potential terms. These quantities, which are generally well determined in a phenomenological analysis,^{1,37} are given in Table III. The radius of the potential well, as already ascertained in previous analyses,^{5,6,12,38}

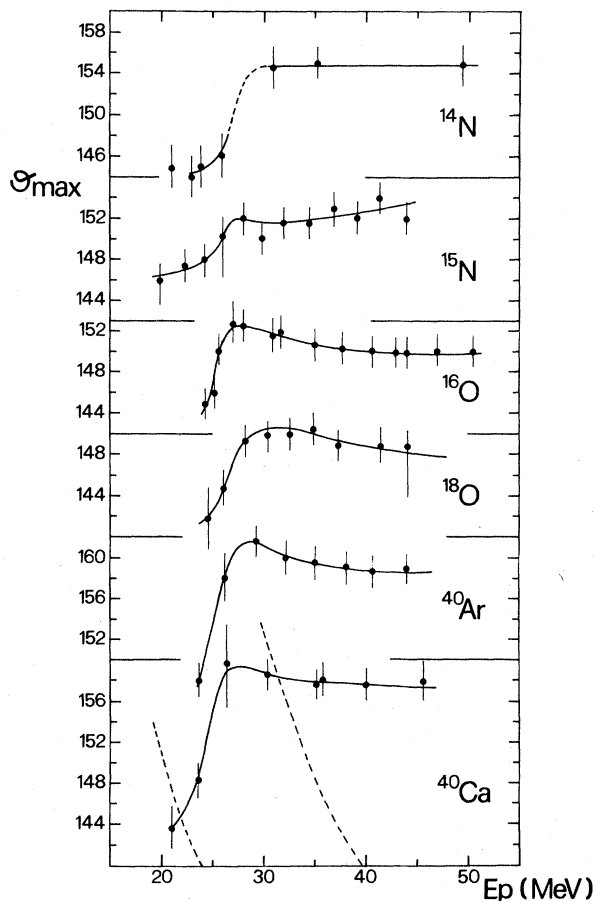


FIG. 6. Angular position of the backward maximum in the angular distribution plotted against the incident energy. The error bars give the estimated uncertainty, while the solid lines serve only to guide the eye. The dashed lines, given for ^{40}Ca , show the energy dependence predicted by an optical-model calculation.

displays a marked decrement with decreasing mass number. The values for the rms, $\langle r^2 \rangle_{\text{OM}}^{1/2}$, deduced in the present analysis are given in column 4 of Table III. These can be compared with the corresponding values for the electric charge distribution³⁹ given in column 5. The difference $\Delta = (\langle r^2 \rangle_{\text{OM}} - \langle r^2 \rangle_{\text{ch}})^{1/2}$, which should be connected with the range of the nucleon-nucleon force, is given in column 6. The resulting values are similar to those determined for heavier nuclei.¹

The volume integrals for the real and imaginary central parts are also given in Table III and are plotted as solid lines in Fig. 10. The dots in this figure show the values obtained with the geometrical parameters fixed at the values in Table II and searching on the well depths. The fluctuations relative to the average trend are generally about

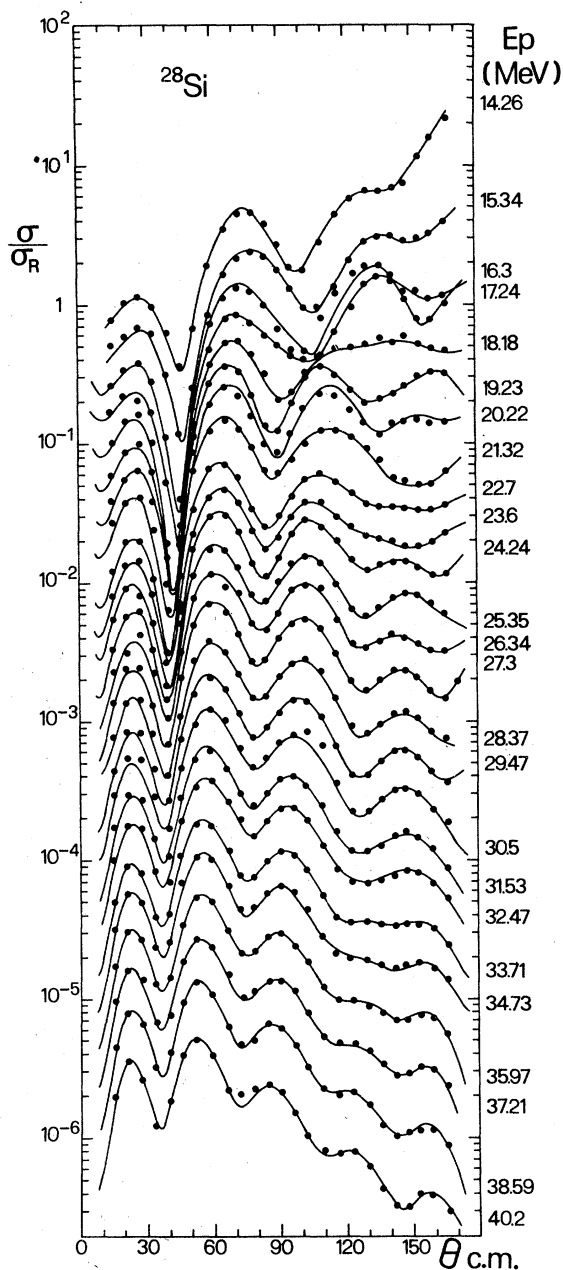


FIG. 7. Differential cross sections for proton elastic scattering on ^{28}Si ; see caption for Fig. 1. The normalization factor is $\exp[0.554(E_p - 14.26)]$.

1–2% for the real part and about 3–5% for the imaginary term. For most cases the energy dependence of the real well depth is in good agreement with that of heavier nuclei. Similar agreement is found also for the absolute values of the volume integrals per nucleon. The larger value for this quantity in the case of the lighter nuclei can be explained as a consequence of the finite

TABLE II. Average energy-dependent optical-model parameters from least-square searches. χ^2 and χ_{tot}^2 give the chi-squares per point, evaluated in the angular range indicated in column 3 and in the full angular range, respectively. The quoted values correspond to the assumption of a 5% error in the experimental points.

Nucleus	Energy range (MeV)	Angular range (deg)	V_0 (MeV)	R_0 (fm)	a_0 (fm)	W_V (MeV)	W_D (MeV)	R_W (fm)	a_W (fm)	V_{so} (MeV)	R_{so} (fm)	a_{so} (fm)	χ^2	χ_{tot}^2
^{12}C	16–20	16°–100°	67.4–0.40E	1.064	0.623	0	4 + 0.1E	1.20	0.60	6.4	1.00	0.575	14	45
	20–40						5.8 + 0.007E						3.8	29
^{15}N	18–22	16°–105°	60.4–0.26E	1.080	0.662	0.06E	0.6 + 0.15E	1.46	0.55	5.8	0.92	0.60	5.4	26
	22–44						4.1–0.01E						5.5	51
^{18}O	14–25	16°–103°	59.5–0.29E	1.100	0.700	0	6.13	1.30	0.67	4.4	1.00	0.60	6.0	11
	25–44						10.4–0.17E						3.8	23
^{24}Mg	15–22	16°–130°	55.9–0.30E	1.144	0.690	0	4.4 + 0.073E	1.32	0.657	5.9	1.01	0.60	12	18
	22–50						10.0–0.18E						7	16
^{28}Si	14–40	15°–124°	56.0–0.30E	1.148	0.663	0.16E–2.0	6.6–0.10E	1.33	0.60	6.3	1.02	0.68	10	34
	21–49	20°–130°	59.1–0.30E	1.140	0.750	0.23E–4.0	10.0–0.156E	1.30	0.66	4.45	1.01	0.56	7.4	19
^{40}Ca	21–48	10°–130°	56.2–0.31E	1.180	0.700	0.10E–2.1	7.4–0.05E	1.30	0.60	5.89	1.05	0.70	9.4	30
													5.3	29

^d Reference 10.

^e Reference 8.

^f Reference 13, for $E > 30$ MeV only.

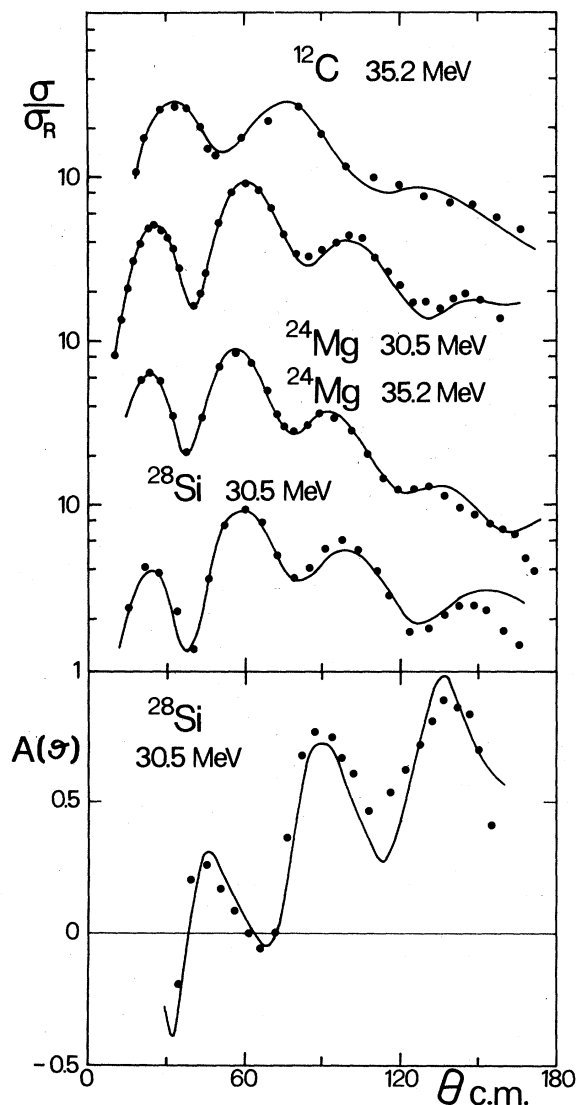


FIG. 8. Proton elastic scattering cross sections at incident energies of 30–35 MeV and optical-model fits, obtained with standard energy averaged optical-model potentials (Table II). The agreement is typical of deformed nuclei.

range and density dependence of the effective nucleon-nucleon force.^{14,15} At $E_p = 35$ MeV, for instance, J_v/A results to be 443 and 405 MeV fm³ for ¹²C and ⁴⁰Ca, respectively, in reasonable agreement with folding model predictions.¹⁴ The volume integrals for the imaginary terms J_w/A given in column 3 of Table III, are in satisfactory agreement with the value of 115 ± 15 MeV fm³ given by Agrawal and Sood³⁷ for nuclear masses $A = 40$ –208. The increment predicted by folding model for lighter nuclei is also verified in this case.

A few anomalies are however apparent. The

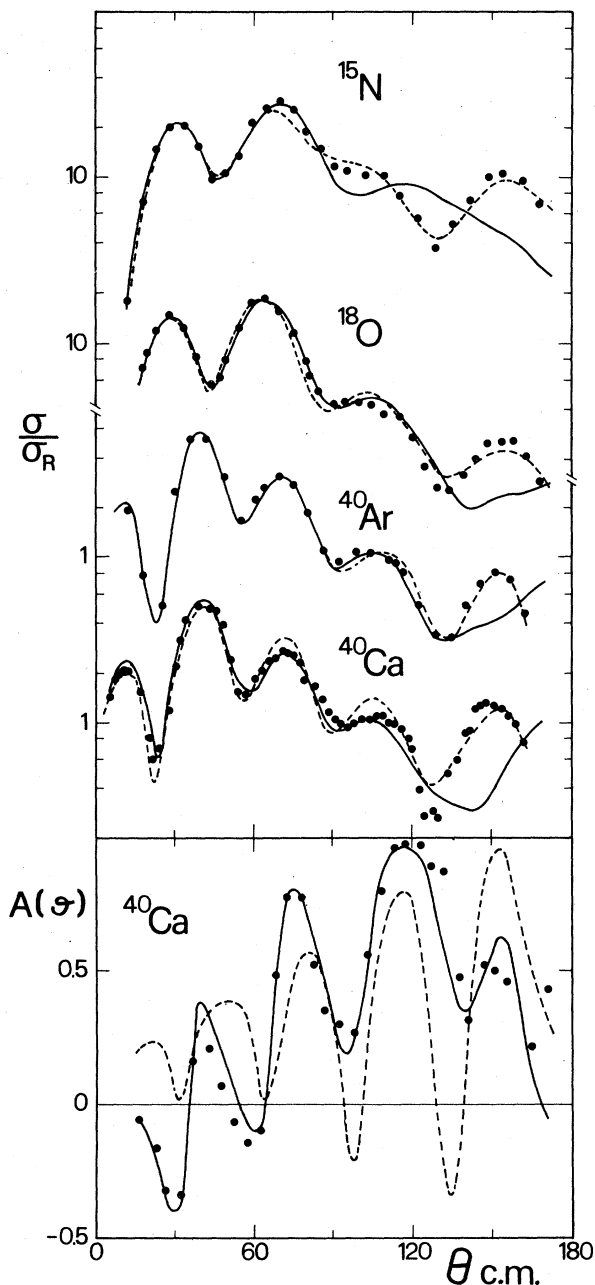


FIG. 9. Proton differential cross sections and optical-model fits, at 35 MeV, given as examples of elastic scattering on spherical light-medium-weight nuclei. The solid lines give the fits obtained by using standard parameters (Table II), while the dashed lines give the results obtained using nonconventional potentials, characterized by a large value for the imaginary and spin-orbit well radius (sets 1 to 4 in Table IV).

real part of the optical-model potential for ¹⁵N shows a weaker energy dependence than that generally found. The radius for the imaginary term for the same nucleus turns out to be rather large.

TABLE III. Volume integrals per nucleon J_v/A and J_w/A for the real and imaginary central parts of the optical-model potentials given in Table II. The optical-model and electric charge rms radii also shown. The quantity Δ is defined by the relationship $\Delta = (\langle r^2 \rangle_{\text{OM}} - \langle r^2 \rangle_{\text{ch}})^{1/2}$.

Nucleus	J_v/A (MeV fm ³)	J_w/A (MeV fm ³)	$\langle r^2 \rangle_{\text{OM}}^{1/2}$ (fm)	$\langle r^2 \rangle_{\text{ch}}^{1/2}$ (fm)	Δ (fm)
¹² C	560(1 - 5.93 10 ⁻³ E)	127 + 0.15E	2.99	2.45	1.71
¹⁵ N	513(1 - 4.31 10 ⁻³ E)	106 + 0.71E	3.12	2.65	1.81
¹⁸ O	525(1 - 5.05 10 ⁻³ E)	134 + 0.67E	3.43	2.76	2.04
²⁴ Mg	502(1 - 5.36 10 ⁻³ E)	100 - 0.08E	3.62	3.04	1.97
²⁸ Si	482(1 - 5.35 10 ⁻³ E)	100 - 0.04E	3.66	3.12	1.91
⁴⁰ Ar	501(1 - 5.07 10 ⁻³ E)	131 - 0.17E	4.11	3.47	2.20
⁴⁰ Ca	502(1 - 5.52 10 ⁻³ E)	94 + 0.30E	4.07	3.47	2.12

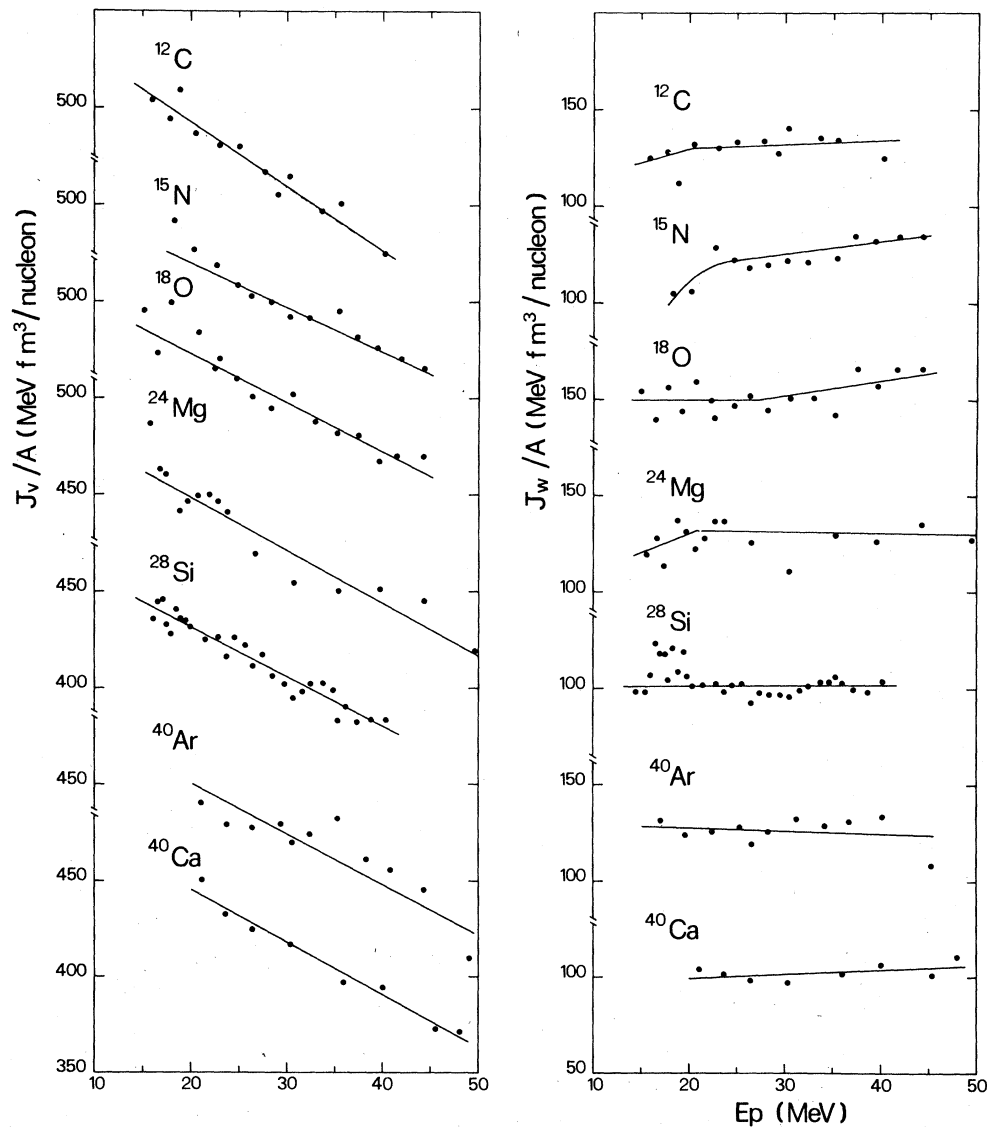


FIG. 10. Values for the volume integral per nucleon of the real and imaginary central parts ($J_v/A, J_w/A$) of the proton optical-model potentials as a function of the incident energy. The solid lines are from the energy-averaged optical potentials in Table II.

In the next section it will be shown that a large radius for the imaginary well can improve the agreement between calculated and experimental differential cross sections, when "unconventional" shapes are found. In paper II it will also be shown that for spherical nuclei in the oxygen region the enhanced yield is not limited at backward angles. Finally, the volume integral of the imaginary terms for ^{24}Mg and ^{18}O proves to be relatively large also in comparison with the lighter nucleus ^{15}N . This large value is found also, for all the strongly deformed nuclei in the $2s-1d$ shell, as is shown in paper II.

For several features, the potentials listed in Table II are very similar to those determined by phenomenological analyses of proton scattering on medium-weight or heavy nuclei. The differences found can be justified in most cases on the basis of the results of folding model calculations. It can therefore be concluded that for light nuclei the differential cross sections at forward angles, where the potential scattering is large, can always be fitted by a conventional optical-model calculation. The cross sections at backward angles instead are reproduced reasonably well only in the case of collective nuclei. In this connection it would be interesting to ascertain whether or not this failure of the model for spherical nuclei is due to some peculiar assumption, such as the analytical form taken for the radial dependence of the potentials.

V. NONCONVENTIONAL OPTICAL-MODEL POTENTIALS

One of the constraints of conventional optical-model analyses concerns the radial dependence assumed for the different terms of the optical potentials. Efforts to improve the fits to scattering data for light nuclei by using nonstandard form factors have already been reported in early

studies.⁴⁰ The Woods-Saxon radial distributions have generally been retained, while attempts were made by using nonstandard values for the parameters, usually the radii of various terms. In Fig. 9 the dashed curves, which are in satisfactory agreement with the differential cross sections, were obtained by assuming a very large value for both or at least one of the radii for the imaginary central and spin-orbit terms (Table IV). However, as already pointed out, the same calculation fails to fit polarization data. It can be observed that a very large spin-orbit radius does not have any clear physical meaning and that its use is probably an indirect way of introducing a sizable l dependence into the optical potential. An l dependence can be justified as due to strong coupling with particular reaction channels.¹⁸ A large value for the radius in the absorptive part of the optical potential can be justified instead by folding model calculations.¹⁵

Free choice of the analytic formula describing the radial dependence of the different terms in the optical potential could cause new ambiguities that would be too large. An indication, which has been tested successfully for the anomalous large angle scattering (ALAS) of alpha particles,⁴¹ can be taken from the folding model. The form factor for the real central term turns out, in fact, to be more diffused¹⁵ than conventionally assumed and can be better described by a squared Woods-Saxon distribution, i.e.,

$$V(r) = V_0(1 + \exp(r - R_0 A^{1/3})/na_0)^{-n} \quad \text{with } n \approx 2.$$

A further indication concerns the imaginary term which, at the incident energies that are most significant for the present study (25–40 MeV), can be reasonably well described by a simple Woods-Saxon distribution, which, however, has a radius larger than that usually assumed.¹⁵ Moreover the radial distribution of the spin-orbit

TABLE IV. Nonconventional optical-model potential parameters.

Set	Nucleus	Energy (MeV)	Form factor	V_0 (MeV)	R_0 (fm)	a_0 (fm)	W_V (MeV)	W_D (MeV)	R_W (fm)	a_W (fm)	V_{so} (MeV)	R_{so} (fm)	a_{so} (fm)
1	^{15}N	35.2	SW	47.7	1.095	0.523	4.98	8.11	1.066	0.373	6.02	1.643	0.766
2	^{18}O	35.2	SW	49.0	1.108	0.746	4.03	2.43	1.611	0.579	2.92	1.154	0.463
3	^{40}Ar	35.2	SW	51.34	1.127	0.773	4.26	3.63	1.352	0.767	3.89	1.284	0.540
4	^{40}Ca	35.8	SW	48.15	1.137	0.823	8.80	3.37	1.303	0.356	3.77	1.459	0.509
5	^{40}Ca	21.1	SW	48.53	1.234	0.682	1.23	6.20	1.371	0.600	5.83	1.050	0.700
6		26.3	$\text{SW}^{1.75}$	50.0	1.317	0.568	2.44	2.72	1.556	0.584	5.83	1.050	0.700
7		30.3	$\text{SW}^{2.0}$	50.94	1.373	0.486	2.61	3.89	1.479	0.605	5.83	1.050	0.700
8		35.8	$\text{SW}^{2.0}$	51.44	1.310	0.496	4.63	0.73	1.572	0.600	5.83	1.050	0.700
9		40.0	$\text{SW}^{2.0}$	49.63	1.370	0.578	3.79	1.41	1.536	0.702	5.83	1.050	0.700
10		45.5	$\text{SW}^{2.0}$	45.46	1.330	0.552	3.41	0.23	1.668	0.554	5.83	1.050	0.700

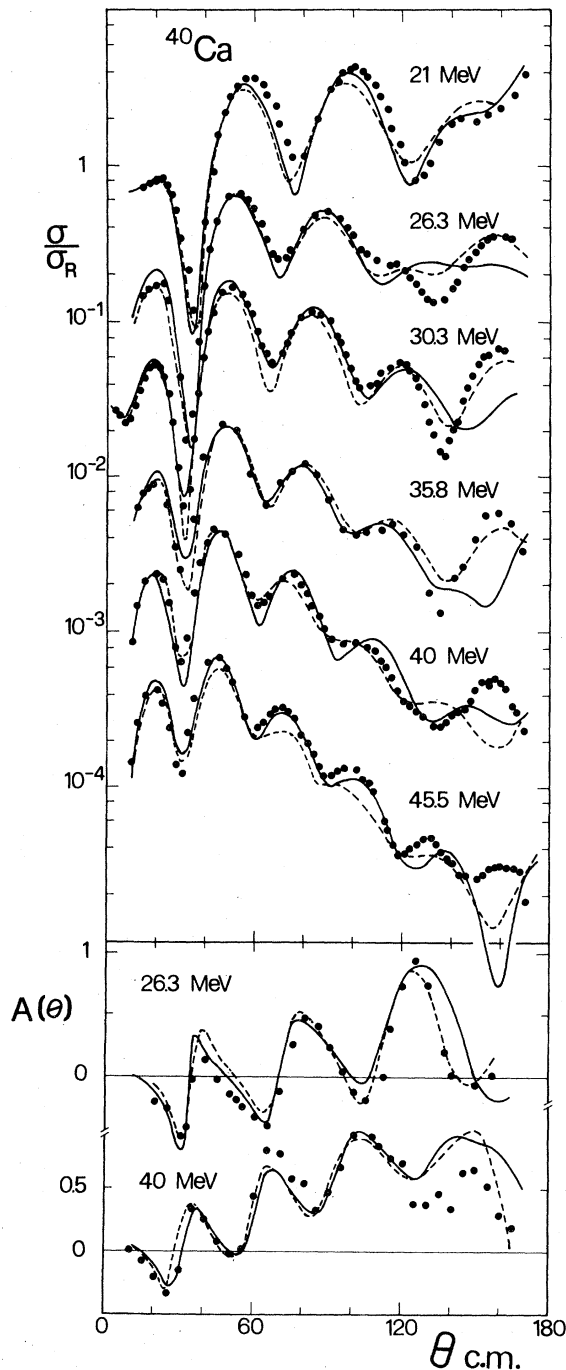


FIG. 11. ^{40}Ca differential cross sections, polarizations, and optical-model fits. The solid lines show the results obtained by a conventional energy-averaged optical-model potential given in Table II. The dashed lines are the fits obtained by a least-squares procedure to cross-section and polarization data, performed at each incident energy by using Woods-Saxon exponential form factors for the real well and a large radius for the imaginary well (sets 5 to 10 in Table IV).

term, as resulting from folding model calculations, does not differ very much from standard-type form factors.¹⁵

We therefore decided to use only radial distributions suggested by the more complete folding model calculations and to test our calculations on complete sets of experimental data, including polarizations, as available for ^{16}O and ^{40}Ca . Standard type radial form factors were used for the spin-orbit and the imaginary term. For the latter, however, a large value for the radius up to $R_w = 1.7$ fm, was allowed in the search. The spin-orbit term was fixed at an average energy-independent value. The real term was assumed to have the form of an exponential of a Woods-Saxon distribution. The search for the best fit exponent was made by analyzing a grid of possible values. For each exponent value n , readjustments are needed of the other parameters, especially large readjustments for the well depth V_0 and diffuseness a_0 . A description is being given here of the results of the analysis of ^{40}Ca data which can be considered only partially successful. The following indications were obtained: (i) The results for polarization data are not appreciably affected. (ii) No modification of the radial shape is required at 21.1 MeV, while exponents between 1 and 2 give limited improvement at 26 MeV, as shown in Fig. 11. (iii) An increased yield, leading to appreciable improvement in the fits at backward angles in the energy range 30–35 MeV can be obtained with an exponent $n = 2$ at the expense, however, of the quality or the fits at forward angles. (iv) No improvements are obtained at higher energies. The latter failure is connected with the same difficulty encountered in conventional optical-model analyses. As stated in Sec. III, it is very difficult for these calculations to reproduce the energy independence of the angular position of the backward maximum. The very large adjustment of the imaginary radius and the real well diffuseness, made by using a squared Woods-Saxon form factor, produces improved fits over a sizable, but still limited, energy range. The fits to energy dependence thus obtained are moreover not substantially improved in comparison to those obtained with no adjustable parameters in a recent folding model calculation by Brieva.¹⁵

VI. PHASE-SHIFT ANALYSIS AND ANGULAR-MOMENTUM LOCALIZATION

This analysis, which is model independent, was performed to ascertain if some particular partial wave could be held responsible for the effect observed. The starting sets of phase shifts used in the search were obtained from the average optic-

al-model potentials of Sec. IV. To minimize ambiguities, which could be further reduced if polarization data were available at each incident energy, other average optical-model potentials^{1,12} were also used to obtain additional starting sets of phase shifts. Moreover the partial waves for each L value up to 9 were first searched separately, so that, for every nucleus and incident energy, those waves could be found which have the largest effect in decreasing the initial χ^2 . Curves like those in Fig. 12 are obtained. As can be seen, the minimum χ^2 value reached is of the same order for all the nuclei. For the nuclei which show the effect, the starting values are much larger and consequently the decrease in χ^2 values obtained in the best fit search is much more marked. For energies above 26 MeV the corresponding variations in the real part of the phase shifts are of the order of 1° or 2° . Larger variations, up to 20%, are found for the factors $\nu = \exp(-2\beta_L)$, where β_L is the imaginary part of the phase shift; their

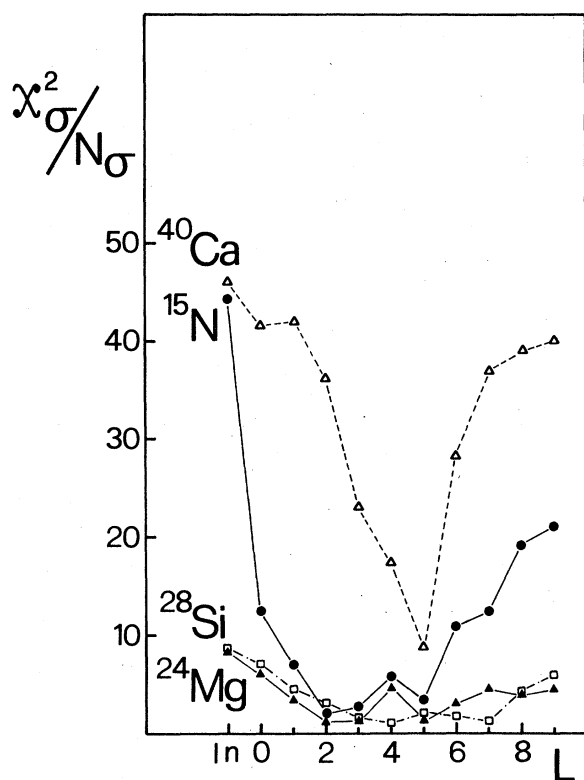


FIG. 12. Results of a best fit procedure to the experimental elastic cross sections, for the nuclei indicated in the figure, at 35.2-MeV proton energy. The partial waves for each L value up to 9 have been separately searched on to find out which waves have the largest effect on the initial χ^2 value (indicated with L in the figure).

signs change for different L values and starting potentials. No regular behavior respect to the incident energy seems to emerge.

Then, for each angular distribution, every partial wave was allowed to vary, starting with the one with the largest effect in χ^2 and proceeding in order of decreasing effect. The fits obtained in these searches are really excellent (Figs. 1-5, 7). The waves involved start being $L=3$ for ^{15}N below 26 MeV and gradually shift to $L=5$ and 6 as the energy and mass increase. In this connection it can be recalled that at 35 MeV, for instance, the angular momentum of the grazing wave rises from about $L=3$ to about $L=5$ while going from ^{15}N to ^{40}Ca . If the average angular momentum is defined as $\langle L \rangle = (\sum_i L_i / \chi_i^2) / (\sum_i 1 / \chi_i^2)$,

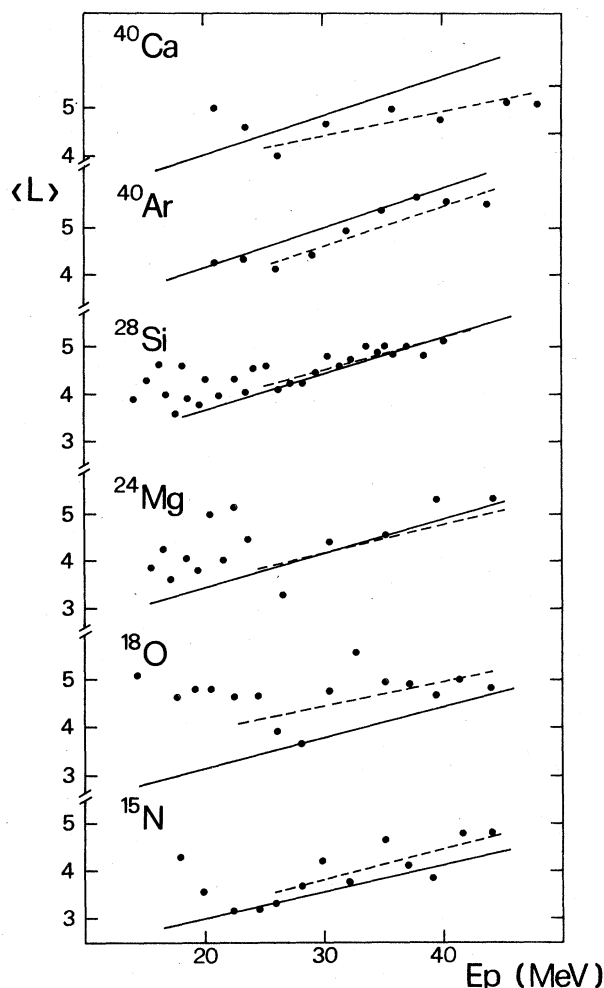


FIG. 13. Average (see text) angular momentum $\langle L \rangle$ of the partial waves involved in the backward yield. The average values are compared with the angular momentum of the grazing wave $L = kR_{eq}$ (solid lines). The dashed lines interpolate the $\langle L \rangle$ values between 26 and 44 MeV.

where χ_i^2 is the chi-square value reached by varying the phase shifts for the partial waves with $J_i = L_i \pm \frac{1}{2}$ and the $\langle L \rangle$ are plotted against the incident energy, the graphs in Fig. 13 are obtained. The uncertainty in these values is of the order of one or two units since low chi-square values are usually reached by more than one partial wave. The $\langle L \rangle$ values can be compared with kR_{eq} , where k is the incident proton wave number and R_{eq} is the uniform sphere equivalent radius defined as $R_{\text{eq}}^3 = R_0^3 A [1 + (\pi a_0 / R_0 A^{1/3})^2]$ in which R_0 and a_0 are the radius and diffuseness parameters for the real well in the optical-model potential used in the search to give the starting set of phase shifts. Below 26 MeV the $\langle L \rangle$ values are larger than kR_{eq} and fluctuate strongly, probably also because of resonant processes.⁵⁻¹⁰ The dashed lines, which interpolate the $\langle L \rangle$ values between 26 and 44 MeV, follow the kinematic increase rather closely. It should be noted that the quality of the agreement between the $\langle L \rangle$ values and kR_{eq} , which is always fairly good in view of the above mentioned uncertainty in the $\langle L \rangle$ values, does not differ for nuclei in which the backward effect is or is not present. In spite of the ambiguities which cannot be avoided completely in this kind of analysis, we can fairly confidently draw the following conclusions: (a) Values of χ^2 that are also an order of magnitude smaller are obtained with small adjustments of the phase shifts concerned. (b) two or more partial waves with L values close to the momentum of the grazing wave are involved. (c) resonant processes entailing a specific intermediate state are ruled out. It can be stated here that a similar

conclusion is obtained in the analysis of the data collected as a function of the mass (see Paper II).

VII. CONCLUSIONS

Angular distributions, similar to those found in the past for ^{16}O and ^{40}Ca , are also displayed by the cross sections for proton scattering on other neighboring nuclei such as ^{15}N , ^{18}O , and ^{40}Ar . A deep minimum followed by a very pronounced maximum appears in the angular distribution at backward angles at a proton energy of about 26 MeV. The effect, present for all the spherical nuclei studied, is more evident at 30–40 MeV and determines an angular distribution shape which cannot be reproduced by optical model calculations with standard geometries. For this model it is especially difficult to account for the energy dependence of the effect, since the experimental angular position of the backward maximum virtually does not depend upon the incident energy.

An extensive phase shifts analysis confirms that only small changes of the phase shifts are required to reproduce the effect. These small adjustments concern mainly the grazing waves.

Finally, the difference between the phenomenological aspects of proton scattering on spherical (^{15}N , ^{16}O , ^{40}Ar , ^{40}Ca) and deformed nuclei (^{12}C , ^{24}Mg , ^{28}Si) is so large as to make clear the value of further systematic studies of proton scattering on light nuclei at an energy of about 35 MeV. These have been performed and are described in paper II.

¹F. D. Becchetti and G. W. Greenlees, *Phys. Rev.* **182**, 1190 (1969).

²J. K. Dickens, D. A. Haner, and C. N. Waddell, *Phys. Rev.* **132**, 2159 (1963).

³O. Karban, P. D. Greaves, V. Hnizdo, J. Lowe, N. Berovic, H. Wojciechowski, and G. W. Greenlees, *Nucl. Phys.* **A132**, 548 (1969).

⁴W. T. H. van Oers and J. M. Cameron, *Phys. Rev.* **184**, 1061 (1969).

⁵R. Sprickmann, K. T. Knopfle, D. Ingham, M. Rogge, C. Mayer-Böricke, and H. V. v. Geramb, *Z. Phys.* **A274**, 339 (1975).

⁶R. De Leo, G. D'Erasmus, F. Ferrero, A. Pantaleo, and M. Pignanelli, *Nucl. Phys.* **A254**, 156 (1975).

⁷I. Lovas, M. Rogge, U. Schwinn, P. Turek, D. Ingham, and C. Mayer-Böricke, *Nucl. Phys.* **A286**, 12 (1977).

⁸R. De Leo, G. D'Erasmus, A. Pantaleo, G. Pasquariello, G. Viesti, M. Pignanelli, and H. V. v. Geramb, *Phys. Rev. C* **19**, 646 (1979).

⁹C. R. Lamontagne, B. Frois, R. J. Slobodrian, H. E. Conzett, C. Leemann, and R. De Swiniarski, *Phys.*

Lett. **45B**, 465 (1973); R. Roy, C. R. Lamontagne, R. J. Slobodrian, J. Arvieux, J. Birchall, R. M. Larimer, and H. C. Conzett, in *Proceedings of the International Conference on Nuclear Structure, Tokyo, 1977*, edited by T. Marumori (Physical Society of Japan, Tokyo, 1978), p. 492.

¹⁰R. De Leo, G. D'Erasmus, A. Pantaleo, G. Pasquariello, G. Viesti, M. Pignanelli, and H. V. v. Geramb, *Phys. Rev. C* **20**, 13 (1979).

¹¹E. E. Gross, R. H. Bassel, L. N. Blumberg, B. J. Morton, A. Van Der Woude, and A. Zucker, *Nucl. Phys.* **A102**, 673 (1967).

¹²B. A. Watson, P. P. Singh, and R. E. Segel, *Phys. Rev.* **182**, 977 (1969).

¹³W. T. H. van Oers, *Phys. Rev. C* **3**, 1550 (1971).

¹⁴C. Mahaux, *Microscopic Optical Potentials, Lecture Notes in Physics*, edited by H. V. v. Geramb (Springer, New York, 1979), Vol. 89, p. 1; J. P. Jeukenne, A. Lejeune, and C. Mahaux, *Phys. Rev. C* **15**, 10 (1977); **16**, 80 (1977).

¹⁵F. A. Brieva and J. R. Rook, *Nucl. Phys.* **A291**, 299

- (1977); A291, 317 (1977); A297, 206 (1978); F. A. Brieva, *Microscopic Optical Potentials, Lecture Notes in Physics*, edited by H. V. v. Geramb (Springer, New York, 1979), Vol. 89, p. 84.
- ¹⁶F. A. Brieva, H. V. v. Geramb, and J. R. Rook, *Phys. Lett.* 79 B, 177 (1978).
- ¹⁷C. L. Rao, M. Reeves III, and G. R. Satchler, *Nucl. Phys.* A207, 182 (1973); P. W. Coulter, and G. R. Satchler, *ibid.* A293, 269 (1977).
- ¹⁸R. S. Mackintosh, and A. M. Kobos, *Phys. Lett.* 62B, 127 (1976); R. S. Mackintosh and L. A. Cordero, *ibid.* 68B, 213 (1977).
- ¹⁹E. Fabrici, S. Micheletti, M. Pignanelli, F. G. Resmini, R. De Leo, G. D'Erasmus, and A. Pantaleo, *Phys. Rev. C* 21, 844 (1980), following paper.
- ²⁰R. De Leo, G. D'Erasmus, E. Fabrici, S. Micheletti, A. Pantaleo, M. Pignanelli, and F. G. Resmini, Report No. INFN/BE-78/8, 1978.
- ²¹L. N. Blumberg, E. E. Gross, A. Van Der Woude, A. Zucker, and R. H. Bassel, *Phys. Rev.* 147, 812 (1966).
- ²²R. M. Craig, J. C. Dore, G. W. Greenlees, J. Lowe, and D. L. Watson, *Nucl. Phys.* 79, 177 (1966).
- ²³J. L. Escudié, R. M. Lombard, M. Pignanelli, F. G. Resmini, and A. Tarrats, *Compte Rendu d'Activité*, Report No. CEA-N-1522, 1971.
- ²⁴J. Stevens, H. F. Lutz, and S. F. Eccles, *Nucl. Phys.* 76, 129 (1966).
- ²⁵J. L. Escudié, R. M. Lombard, M. Pignanelli, F. G. Resmini, and A. Tarrats, *Phys. Rev. C* 10, 1645 (1974).
- ²⁶J. Eenmaa, R. K. Cole, C. N. Waddell, H. S. Sandhu, and R. R. Dittman, *Nucl. Phys.* A218, 125 (1974).
- ²⁷V. E. Lewis, E. J. Burge, A. A. Rush, D. A. Smith, and N. K. Ganguly, *Nucl. Phys.* A101, 589 (1967); A. A. Rush, E. J. Burge, V. E. Lewis, D. A. Smith, and N. K. Ganguly, *ibid.* A104, 340 (1973).
- ²⁸G. M. Crawley and G. T. Garvey, *Phys. Rev.* 160, 981 (1967).
- ²⁹A. G. Blair, C. Glashauser, R. De Swiniarski, J. Goudergues, R. Lombard, B. Mayer, J. Thirion, and P. Vagonov, *Phys. Rev. C* 1, 444 (1970).
- ³⁰R. De Swiniarski, H. E. Conzett, C. R. Lamontagne, B. Frois, and R. J. Slobodrian, *Can. J. Phys.* 51, 1293 (1973).
- ³¹R. De Swiniarski, F. G. Resmini, D. L. Hendrie, and A. D. Bacher, *Nucl. Phys.* A261, 111 (1976).
- ³²A. A. Rush, E. J. Burge, and A. D. Smith, *Nucl. Phys.* A166, 378 (1971).
- ³³K. H. Bray, K. S. Jayaraman, G. A. Moss, W. T. H. van Oers, D. O. Wells, and Y. I. Wu, *Nucl. Phys.* A167, 57 (1971).
- ³⁴D. L. Watson, J. Lowe, J. C. Dore, R. M. Craig, and D. L. Baugh, *Nucl. Phys.* A92, 193 (1967).
- ³⁵H. F. Lutz, D. W. Heikkinen, and W. Bartolini, *Nucl. Phys.* A198, 257 (1972).
- ³⁶M. Pignanelli, S. Micheletti, I. Iori, P. Guazzoni, F. G. Resmini, and J. L. Escudié, *Phys. Rev. C* 10, 445 (1974).
- ³⁷D. C. Agrawal and P. C. Sood, *Phys. Rev. C* 11, 1854 (1975).
- ³⁸D. L. Pham and R. De Swiniarski, *Nuovo Cimento* 41A, 543 (1977).
- ³⁹C. W. De Jager, H. De Vries, and C. De Vries, *Atomic Data and Nucl. Data Tables* 14, 479 (1974).
- ⁴⁰N. M. Clarke, E. J. Burge, D. A. Smith, and J. J. Dore, *Nucl. Phys.* A157, 145 (1970).
- ⁴¹H. P. Gubler, U. Kiebele, H. O. Mayer, G. R. Plattner, and I. Sick, *Phys. Lett.* 74B, 202 (1978).